RESEARCH ARTICLE
Cytoskeleton, April 2012 69:235–251 (doi: 10.1002/cm.21018)

Myosin VI is Required for Maintenance of Brush Border Structure, Composition, and Membrane Trafficking Functions in the Intestinal Epithelial Cell

Peter S. Hegan,[1] Hector Giral,[2] Moshe Levi,[2] and Mark S. Mooseker[1,3,4]*

[1]Department of Molecular, Cellular, and Developmental Biology, Yale University, New Haven, Connecticut
[2]Department of Medicine, Division of Renal Diseases and Hypertension, University of Colorado Denver, Aurora, Colorado
[3]Department of Cell Biology, Yale University, New Haven, Connecticut
[4]Department Pathology, Yale University, New Haven, Connecticut

Received 18 November 2011; Revised 26 January 2012; Accepted 6 February 2012
Monitoring Editor: Roberto Dominguez

Characterization of the intestinal epithelium of the *Snell's waltzer* (*sv/sv*) mouse revealed that myosin VI (Myo6) is required for proper brush border (BB) ultrastructure, composition and membrane traffic. The defects observed were distinct from that observed in the myosin Ia KO, even though Myo6 is lost from the BB in this KO. Myo6 is expressed throughout the length of the small and large intestine; it is localized to the subapical inter-microvillar (MV) domain and basolateral membrane. Defects in the BB include apparent lifting of the plasma membrane off of the actin cytoskeleton in the inter-MV region, fusion of MV, and disorganized morphology of the terminal web. The molecular composition of the *sv/sv* BB is altered. This includes increased expression of myosin Va, myosin Ie and the MV actin binding proteins espin and phosphorylated-ezrin; myosin Id is reduced. Changes in endocytic components include reduced clathrin and adaptin β, and increased disabled-2. Endocytic uptake of lumenal lactoferrin is inhibited in adult, but not neonatal intestinal epithelial cells. There is increased BB membrane-associated expression of both the Na^+/H^+ exchanger, NHE3 and the Na^+/phosphate transporter, NaPi2b. These results suggest that Myo6 is involved in the regulated trafficking of NHE3 and NaPi2b between the BB membrane and endosome. © 2012 Wiley Periodicals, Inc

Key Words: unconventional myosin, Snell's waltzer, endocytosis, NHE3, NaPi2b

*Address correspondence to: Mark S. Mooseker, Department of Cell Biology, Yale University, New Haven, CT 06520. E-mail: mark.mooseker@yale.edu

Published online 10 February 2012 in Wiley Online Library (wileyonlinelibrary.com).

Introduction

Myosin VI (Myo6) is unique among characterized members of the myosin family of actin based motors in that it moves toward the minus (pointed) end of the actin filament [Wells et al., 1999] (with the potential exception of myosin IXb which may be bidirectional since a tail-truncated form was reported to be minus-end directed [Inoue et al., 2002]; however, full length Myo9b [O'Connell and Mooseker, 2003], a different truncate of Myo9b [O'Connell et al., 2007], and full length and tail-truncated *Caenorhabditis elegans* Myo9 [Liao et al., 2010] are plus end motors). Given its unique status it is not surprising that Myo6 has been implicated in a broad range of cellular functions. These include clathrin-mediated endocytosis, regulated trafficking of membrane proteins, Golgi organization, actin dynamics, cell migration including tumor cell invasivity and transcription [for reviews see Buss and Kendrick-Jones 2008; Chibalina et al. 2009]. Several Myo6 binding proteins have been identified, shedding light on the molecular basis for its diverse functions. These include clathrin adaptor proteins, Disabled-2 (Dab-2) and GAIP interacting protein, C terminus (GIPC), and also optineurin, a protein involved in exocytic traffic from the Golgi to the basolateral domain of epithelial cells and to the leading edge of migrating cells (for review of these and other binding partners, see Buss and Kendrick-Jones [2008, 2011]).

Phenotypic characterizations of mice homozygous for the Myo6 mutation, *Snell's waltzer* (*sv*) have been particularly useful in defining the in vivo functions for Myo6. Mice homozygous for the *sv* mutation (*sv/sv*) mice are deaf and exhibit constant spinning behavior due to vestibular dysfunction [Deol and Green, 1966]. *Myo6* was identified as the target gene for the *sv* mutation. *Sv/sv* mice are functional nulls for Myo6 and loss of Myo6 expression was shown to result in degeneration of the neurosensory

epithelia of the inner ear [Avraham et al., 1995]. Subsequent electron microscopic studies on inner ear hair cells of neonate *sv/sv* mice, prior to neurosensory epithelial degeneration, revealed that the membranes of adjacent stereocilia were fused at their bases, suggesting a role of Myo6 in tethering the plasma membrane to the underlying stereocilia actin core [Self et al., 1999]. Consistent with such a tethering function, Myo6 is associated with the rootlet end of the stereocilium actin core at the base of the stereocilium [Hasson et al., 1997]. However, Myo6 is also highly concentrated in the pericuticular necklace, a region of the subapical cytoplasm between the cuticular plate and cell junctions [Hasson et al., 1997]. The pericuticular necklace is filled with vesicles, and is the presumed region of endocytic and exocytic traffic at the apical membrane [Hasson et al., 1997]. Thus, the loss of Myo6-dependent functions in this membrane traffic could contribute to hair cell dysfunction. A more recent study demonstrated that formation and function of ribbon synapses within the neurosensory epithelium is also defective in the *sv/sv* mouse, and thus synapse dysfunction could also be a contributor to epithelial degeneration [Roux et al., 2009].

Since the initial phenotypic characterization of the inner ear defects of the *sv/sv* mouse, several other *sv/sv* tissues and cell types that express Myo6 have been examined. Myo6 is a component of the postsynaptic density [Osterweil et al., 2005], and synapse formation in the *sv/sv* hippocampus and in cultured hippocampal neurons is defective. Moreover, AMPA and insulin stimulated endocytic internalization of glutamate receptors is blocked in *sv/sv* hippocampal neurons. However, transferrin uptake is normal in these neurons, indicating that Myo6 function in clathrin-mediated endocytosis is cargo selective, presumably through its association with a select set of clathrin adaptor proteins [Osterweil et al., 2005]. Analysis of the various modes of endocytosis in bone marrow-derived dendritic cells of the *sv/sv* mouse revealed no defects in either clathrin-mediated endocytosis or phagocytosis. Surprisingly, however, there was significant enhancement of fluid phase macropinocytosis, suggesting that Myo6 somehow acts as a "governor" on this form of endocytosis [Holt et al., 2007]. Analysis of *sv/sv* embryonic fibroblasts indicated that the size of the Golgi was reduced compared to that in control fibroblasts, implicating a role for Myo6 in Golgi organization and/or function [Warner et al., 2003]. In the kidney, Myo6 is expressed in the proximal tubule epithelial cell where it is localized to the subapical, inter-microvillar (MV) domain of the brush border (BB) and along the length of MV [Biemesderfer et al., 2002]; other studies have shown that elevated blood pressure results in increased recruitment of Myo6 into the inter-MV domain [Yang et al., 2005]. The *sv/sv* mouse has also been shown to exhibit proteinurea, indicating defects in endocytic uptake of protein from the glomerular filtrate. This was confirmed by demonstrating greatly reduced uptake of lumenal horse radish peroxidase in *sv/sv* proximal tubules as compared to *sv/+* [Gotoh et al., 2010].

In the intestinal epithelial cell (enterocyte) Myo6 is associated with the inter-MV domain of the apical BB [Heintzelman et al., 1994]. In the *sv/sv* enterocyte, cGMP-dependent endocytic trafficking of the cystic fibrosis transmembrane conductance regulator (CFTR) from the apical BB membrane to the apical endosome is defective [Ameen and Apodaca, 2007]. A similar role for Myo6 in CFTR trafficking in airway epithelial cells was demonstrated by expression of a dominant-negative tail domain of Myo6 [Swiatecka-Urban et al., 2004]. In the present study we have conducted a comprehensive analysis of the *sv/sv* enterocyte along the entire length of the intestinal axis. This includes effects on BB ultrastructural organization and molecular composition, BB associated endocytosis of lumenal lactoferrin and regulated trafficking of the Na^+/H^+ exchanger, NHE3 and the Na^+/phosphate (Pi) transporter, NaPi2b.

Materials and Methods

Animals

Mice of the strain B6 × STOCK *Tyrc-ch Bmp5se* +/+ *Myo6sv/J* (stock #000578) were purchased from Jackson Labs (Bar Harbor, ME) and used to develop a breeding colony. Myo6 mutant mice (*sv/sv*) displayed the circling, head tossing, and hyperactivity phenotype that is associated with this deafness mutation. Heterozygous mice (*sv/+*) appear normal and were used as control animals in all experiments described, except for the BB membrane vesicle (BBMV) preparation, for which C57BL/6J (Jackson Labs) WT mice were used. All data shown was generated using male mice. All procedures involving mice were performed in accordance with an approved Yale – IACUC animal protocol.

Electron Microscopy

Tissues were processed for electron microscopy as described in Mooseker and Tilney [1975]. Small and large intestine was dissected and flushed with 4°C phosphate buffered saline (PBS). The gut was everted, and segments of duodenum, jejunum, ileum, and proximal colon were cut into small pieces and fixed in 2% glutaraldehyde, 0.2% tannic acid in 0.1 M sodium phosphate buffer, pH 7.0 for 10 min at room temperature (RT), and then shifted to 4°C for an additional 50 min. Following fixation the tissue was washed three times with 0.1 M sodium phosphate buffer, pH 7.0, and then incubated on ice for 1 h in 1% osmium tetroxide in 0.1 M sodium phosphate buffer, pH 6.0. The tissue was then washed three times with cold water and incubated overnight at 4°C in 1% uranyl acetate. The samples were dehydrated with a 25–

100% ethanol series at RT, followed by two 10 min incubations in propylene oxide. The tissue was embedded in EmBed 812 (Electron Microscopy Sciences [EMS], Hatfield, PA) following established protocol. Imaging was done on a JEOL 1230 transmission electron microscope (JEOL, Tokyo, Japan), and digital images were recorded with a Hamamatsu ORCA-HR digital camera (Hamamatsu, Hamamatsu City, Japan). Quantification of MV length was performed by measuring individual MV from base to tip on each side (*L*1 and *L*2 with *L*2 assigned to the shorter of the two lengths) and by measuring the total actin core bundle length (*L*3). MV length difference between *sv*/+ and *sv*/*sv* is expressed as the mean standard deviation between *L*1 and *L*2 in order to account for the variation of MV length along the long axis of the duodenal villus axis. To assess for variations in total MV core length as a function of MV length, the ratio of *L*3/*L*1 (total MV core length [MV plus rootlet]/MV length) was determined with the assumption that *L*1 is representative of lengths of MV with the least inter-MV perturbation. Microsoft Excel (Microsoft, Redmond, WA) was used to generate statistical data.

Immunofluorescence Microscopy

The intestine was dissected and flushed with ice cold PBS. The gut was everted, and segments of duodenum, jejunum, ileum, and colon were cut into small pieces and fixed with 4% paraformaldehyde (prepared from a freshly opened vial of 16% paraformaldehyde (PFA) from EMS) in PBS for 10 min at RT and then shifted to 4°C for an additional 50 min. The tissue was washed twice with PBS, followed by 30 min in each of 5%, 8%, 12%, and 16% sucrose in PBS at RT. The tissue was incubated overnight in 20% sucrose in PBS at 4°C, and the following day was incubated in 12% sucrose, 35% optimal cutting temperature (OCT) (Sakura Finetek USA, Torrance, CA) in PBS for 1 h at RT. The tissue was embedded in 12% sucrose + 35% OCT in PBS and stored at −80°C. Five micron sections were cut on a Leica CM 3050S cryostat (Leica, Wetzlar, Germany) and mounted on Superfrost + slides (Esco, Portsmouth, NH). The following steps were done with either PBS or TBS-T as the buffer, depending on the primary antibody used. The sections were washed 3 × 5 min with RT PBS to remove OCT. The tissue was blocked for 1 h at RT in 10% normal goat serum (NGS) in PBS. Primary antibodies were diluted in PBS + 5% NGS and incubated at RT for 1 h, or overnight at 4°C. The slides were then washed 3 × 10 min with PBS. Alexa fluor labeled secondary antibodies (Invitrogen, Carlsbad, CA) were diluted 1:200 in PBS containing 5% NGS, 0.33 μM rhodamine phalloidin (Invitrogen) and 1 μg/ml Hoechst dye (Sigma, St. Louis, MO) and incubated for 1 h at RT in the dark. Slides were then washed 3 × 10 min with PBS and coverslips were mounted with Prolong Gold antifade media (Invitrogen). Primary antibodies directed against the following proteins were used in this study for immunofluorescence microscopy: Myo6 [Hasson and Mooseker, 1994], Myo1e [Skowron et al., 1998], espin (Gift of J. R. Bartles, Northwestern University) [Bartles et al., 1996], clathrin and p-ezrin (Cell Signaling Technology, Danvers, MA), NHE3 (Alpha Diagnostic International, San Antonio, TX), Lactoferrin (Sigma), and NaPi2b [Giral et al., 2009]. All primary antibodies were used at 10 μg/ml or a dilution of 1:100. All microscopy was done using a Zeiss (Thornwood, NY) LSM510 META laser scanning confocal microscope, and digital images were captured using ZEN 2009 software (Zeiss). Both *sv*/+ and *sv*/*sv* tissue sections were mounted on the same slide, allowing equal treatment during preparation and were imaged with identical microscope settings. Contrast enhancement, cropping, and all other image manipulation was done using ImageJ (http://rsb.info.nih.gov/ij/; NIH).

BB and BBMV Isolation and Immunoblotting

BBs were purified from the entire length of the small intestine as previously described [Mooseker et al., 1978] except that the sucrose purification step consisted of only 50% (w/w) sucrose in Solution A (75 mM KCl, 2 mM $MgCl_2$, 1 mM EGTA, 10 mM imidazole, pH 7.1) in which the crude BBs were suspended by adding five volumes of 60% sucrose (in Solution A) to one volume of BB suspension in Solution A containing 1 mM dithiothreitol, overlaid with 40% (w/w) sucrose in Solution A. Purified BBs collected at the 40%/50% sucrose interface. Total mucosal protein samples were collected from an aliquot of the initial mucosal homogenate by addition of 50% trichloroacetic acid (TCA) to 5% final concentration, to precipitate protein. TCA precipitates were washed two times in cold water and solubilized in SDS PAGE sample buffer. To assess protein expression levels along the length of the gut axis, equal sized pieces of duodenum, jejunum, ileum, and colon were dissected, mucosa was scraped off and homogenized in 5% TCA, and the precipitates processed for SDS PAGE as described above.

BB membrane vesicles were prepared by the Mg^{2+} precipitation method from ileum mucosa of *sv*/*sv* and WT mice. Ileum scrapes from two mice were combined in 15 ml isolation buffer (50 mM mannitol, 2 mM Hepes/Tris pH 7.1, and Complete, EDTA-free protease inhibitor cocktail [Roche, Mannheim, Germany]). Homogenization, using a Potter-Elvejham pestle attached to a high speed drill was performed with 8–10 rapid strokes and homogenates were transferred to a chilled centrifuge tube. The first Mg^{2+} precipitation step was performed by addition of 200 μl of 1 M $MgCl_2$ to the homogenate and incubation for 20 min. After centrifugation at 3000 × *g* for 20 min the supernatant was sedimented at 38,000 × *g* for 40 min. The resulting pellet was resuspended with precipitation buffer B (300 mM mannitol, 20 mM Hepes/NaOH pH 7.2, 0.1 mM $MgSO_4$ and protease inhibitors) and

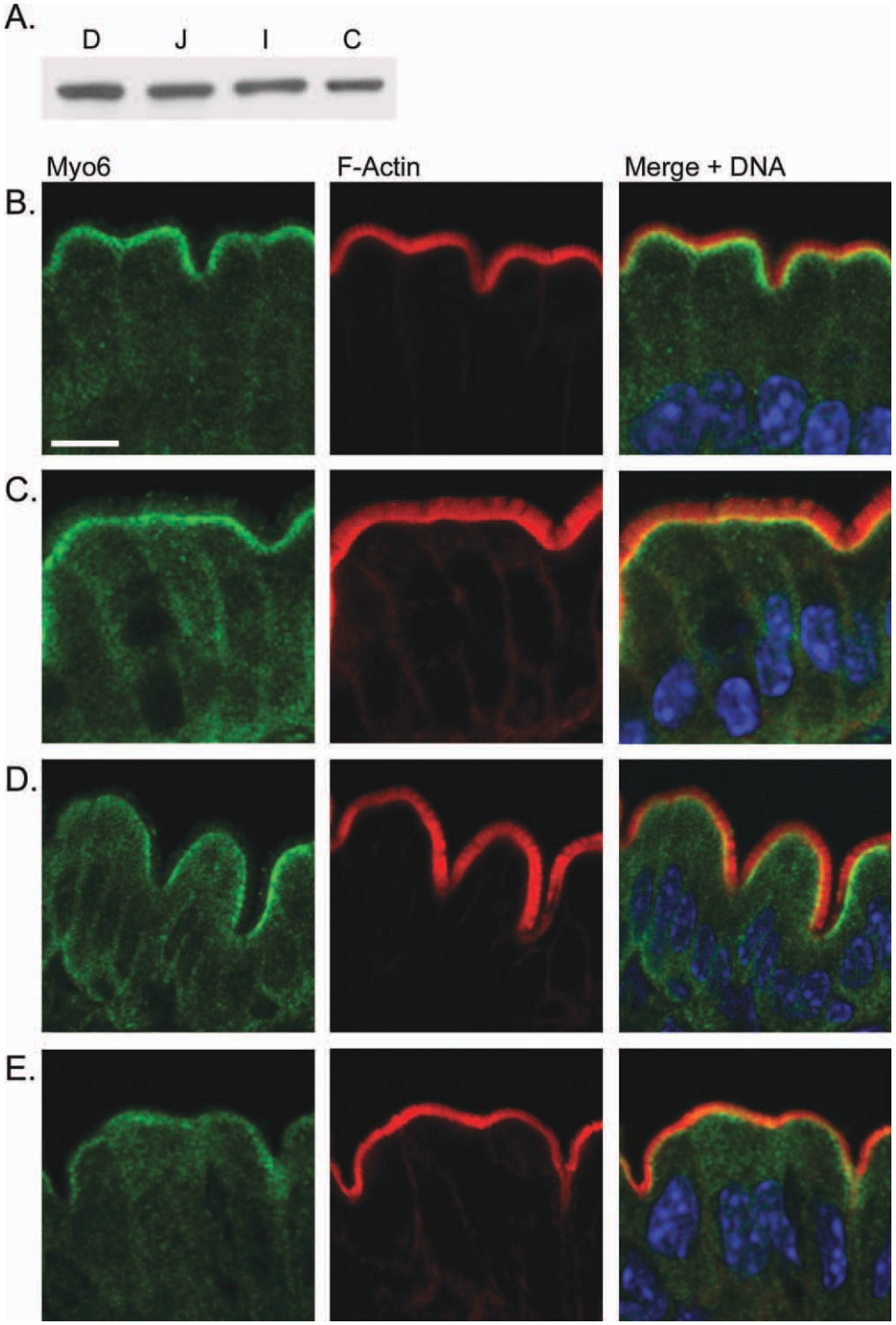

Fig. 1. Myo6 is expressed throughout the small and large intestines and localizes primarily to the inter-MV/terminal web region of the enterocyte. (**A**) Immunoblot analysis indicates that Myo6 is expressed in all regions of the small intestine and in the colon. Expression levels are similar in the duodenum (D), jejunum (J), and ileum (I) of the small intestine, with lesser amounts expressed in the colon (C). (**B–E**) *Sv*/+ mouse intestine stained with Myo6 antibody shows that localization is concentrated to the inter-MV region and terminal web. Lesser amounts of Myo6 are associated with basolateral membrane, MV, and cytoplasm. (B) Duodenum, (C) jejunum, (D) ileum, and (E) proximal colon. Bar = 10 μm.

subjected to a second Mg^{2+} precipitation for 20 min. After centrifugation of the solution at 6000 × *g* for 20 min the supernatant was sedimented at 38,000 × *g* for 40 min. The resulting pellet corresponds to the final BBMV preparation.

All whole cell homogenate (WCH) and BB samples were run on 5–20% gradient gels loaded for equal protein and transferred to Hybond nitrocellulose membrane (GE Healthcare, Piscataway, NJ). Horseradish peroxidase-conjugated secondary antibodies (Pierce, Rockford, IL) were

visualized by Enhanced Chemo Luminescence (GE Healthcare). In addition to the primary antibodies listed above for immunostaining, other primary antibodies used in this study for immunoblot analysis included Myo5a [Espreafico et al., 1992], adaptin β and Dab-2 (BD Biosciences, Franklin Lakes, NJ), beta actin (AC-74; Sigma), Myo1d (Proteintech Group, Chicago, IL), and ezrin (Cell Signaling Technology). All primary antibodies were used at 1 μg/ml or a dilution of 1:1000, except beta actin which was used at a dilution of 1:10,000. To quantify levels of NaPi2b and NHE3 equal volumes of all BB membrane samples were loaded on 5–20% gels and prepared for immunoblot as described above. ImageJ was used to quantify levels of NaPi2b and NHE3, and all samples were normalized based on quantification of beta actin in each BB membrane sample; five to seven separate BB membrane preparations were used per genotype to quantify the protein levels shown in Figs. 5F and 5G. Statistics and histograms were generated with Excel (Microsoft). Data is expressed as arbitrary units (WT = 100) and the results reflect the fold increase seen between WT and *sv/sv*.

Lactoferrin Endocytosis Assay

OPTI-MEM (Gibco/Invitrogen, Carlsbad, CA) media containing 10% fetal bovine serum (Hyclone, Rockford, IL) was pre-equilibrated in a 37°C tissue culture incubator (5% CO_2). Bovine lactoferrin (Sigma) was added to the media at a concentration of 1 mg/ml. For 4°C experiments the dishes were removed from the incubator and chilled on ice until they were cold. Five-month-old adult mice were fasted for 2 h prior to intestinal explant culture. Jejunum was rapidly dissected from *sv/+* and *sv/sv*, flushed with 37°C media to remove lumenal contents, everted, cut into ~2 cm pieces and placed into the culture media. Dissected jejunum was measured and all samples were taken from similar regions for both genotypes. The everted explants were cultured at either 4°C or 37°C for 30 min, washed with media, and then fixed and processed for immunofluorescence microscopy as described above.

Pi Diet Effects on NaPi2b Expression

Low (0.1%) and high (1.2%) Pi mouse diet (0.6% calcium) was purchased from Harlan Teklad (Madison, WI) and fed ad libitum to both *sv/+* and *sv/sv* mice for a minimum of 14 days [Giral et al., 2009]. Mice were then sacrificed and tissue was collected from duodenum, jejunum, proximal ileum, and distal ileum. These tissue samples were fixed and processed for immunofluorescence microscopy of NaPi2b localization as described above.

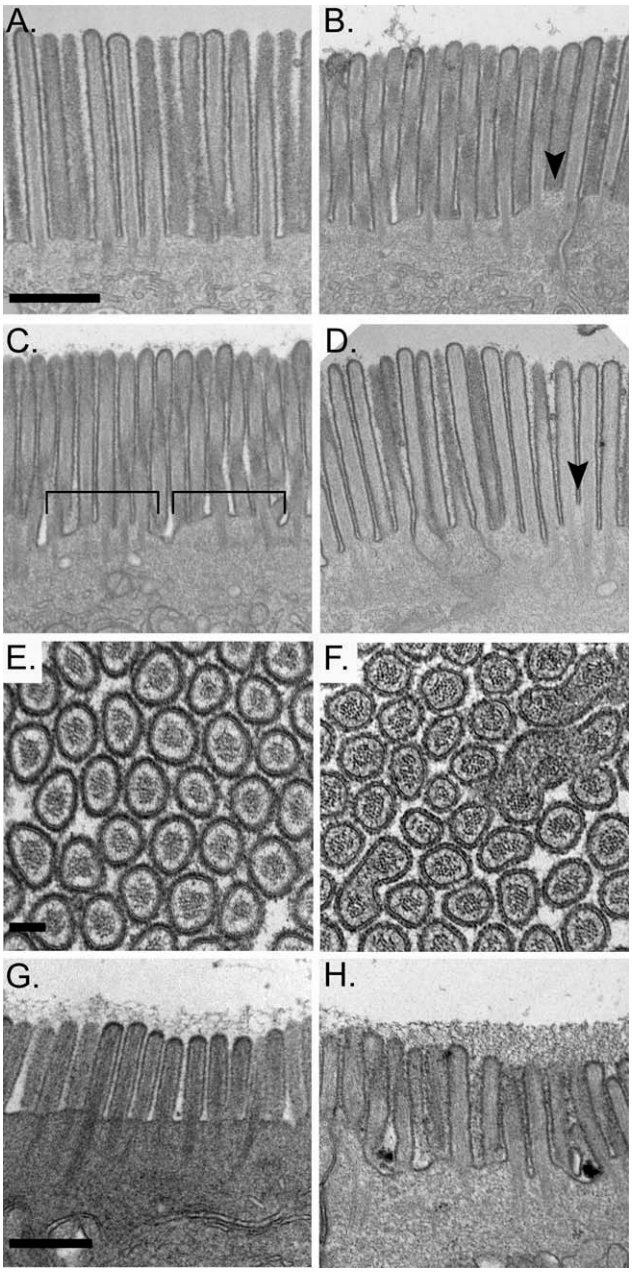

Fig. 2. Enterocyte ultrastructure is disrupted by the loss of Myo6 in whole gut sections. (**A**) Transmission electron microscopy (TEM) of sv/+ duodenum. Note that the microvilli are of uniform length and the cell surface at the base of the MV is uniformly ordered. (**B–D**) Examination of *sv/sv* (B) duodenum, (C) jejunum, and (D) ileum shows that the loss of Myo6 causes the inter-MV membrane to become un-tethered from the underlying cytoskeleton and lift up between microvilli (arrows, B, D), also note that membrane tethering defects involving several MV leads to the formation of "islands" of fused MV (brackets, C) leading to a disorganized appearance of the terminal web region of the cell. (**E**, **F**) Cross sections taken just above the inter-MV region of the enterocyte, note that in *sv/+* (E) all MV are separate from each other, while in *sv/sv* (F) many MV are fused, in groups of 2–4. (**G**, **H**) The inter-MV region of colonic enterocytes is also disrupted in *sv/sv* (H) as compared to *sv/+* (G). Bar A–D = 500 nm, E, F = 100 nm, G, H = 500 nm.

Results

Myo6 is Expressed in Enterocytes from Duodenum to Colon

Myo6 is expressed in approximately equal amounts along the entire length of the small intestine based on immunoblot analysis of equivalent protein concentrations of total WCHs taken from these segments. Expression is lower in the colon as compared to small intestine, but still substantial (Fig. 1A). Myo6 localizes primarily to the subapical/terminal web region of the enterocyte in both small and large intestine. Lesser amounts of Myo6 are visible on basolateral membrane, MV, and there was also diffuse cytoplasmic staining (Figs. 1B–1E).

The Inter-MV Domain of the *sv/sv* BB Exhibits Morphological Perturbations

Ultrastructural examination of the *sv/sv* mouse gut revealed several types of ultrastructural defects along the entire length of the gut (Fig. 2). The loss of Myo6 results in perturbations of the inter-MV region of the BB membrane. In *sv/+* BBs, the position of the inter-MV membrane on either side of the base of the MV is quite regular; in *sv/sv* there are frequent regions where the position of the inter-MV membrane is higher up on the MV core on one (see arrows in Fig. 2) or both sides relative to neighboring MV (brackets in Fig. 2). This apparent membrane detachment at the base of MV is analogous to that seen in *sv/sv* inner ear hair cells [Self et al., 1999]. This perturbation of the inter-MV membrane leads to a general disorganized appearance of the terminal web region as compared to the regularly ordered inter-MV region of the *sv/+* enterocyte (Figs. 2A–2D). Cross sections through the base of MV in the *sv/sv* mouse (Figs. 2E and 2F) show that these inter-MV membrane perturbations result in fusion of MV, with two to four MV cores surrounded by a single MV membrane No such MV fusions were observed in cross sections of MV of the *sv/+* mouse.

To quantify the effect that the loss of Myo6 has on the organization of the inter-MV domain, length measurements were taken from each side of individual MV of longitudinally sectioned BBs in both *sv/+* and *sv/sv* duodenal enterocytes (*L*1 and *L*2 in Fig. 3A). The length of the entire MV core (MV core underneath the MV membrane plus rootlet) (*L*3 in Fig. 3A) was also measured. In *sv/+* enterocytes, the standard deviation between *L*1/*L*2 is quite low, indicative of the essentially straight-line appearance of the inter-MV zone at the base of MV in these enterocytes. In contrast, there was significantly greater standard deviation between *L*1/*L*2 in the *sv/sv* enterocyte, indicative of the apparent lifting/detachment (or failure of attachments to form during BB assembly) of the BB membrane at the base of MV (Fig. 3B). In *sv/+*, as in wild type (WT) enterocytes, MV length is quite uniform within a given

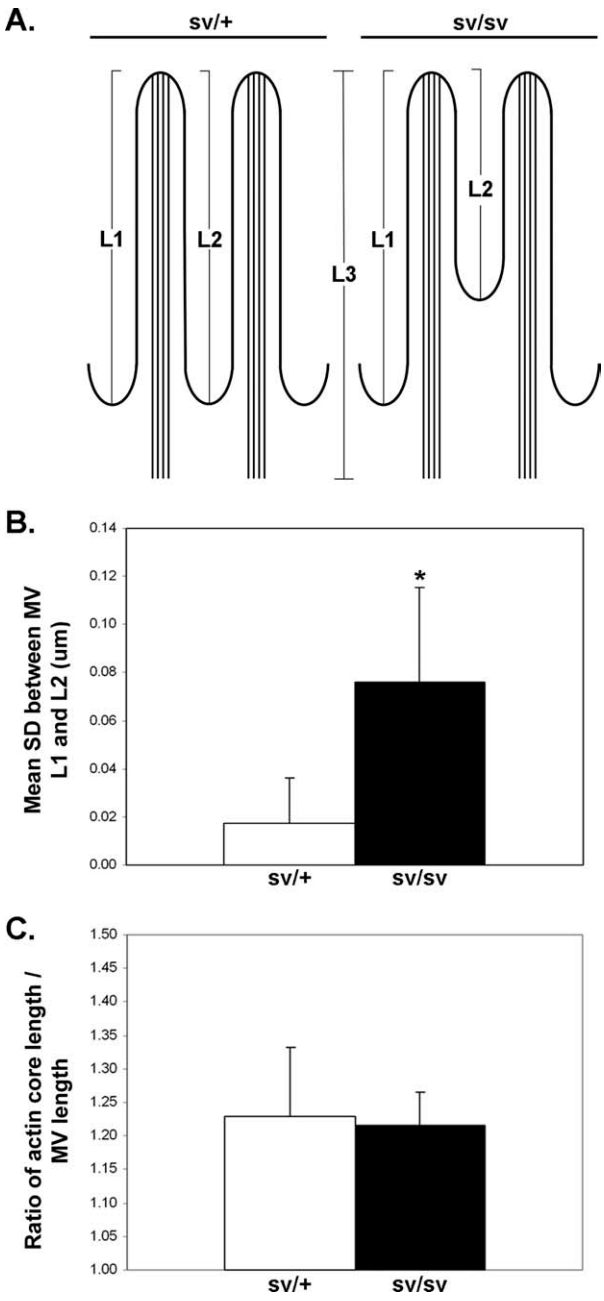

Fig. 3. Loss of Myo6 results in variations of MV base to MV tip lengths within individual MV but not in total MV core length. (**A**) Schematic representation of how MV length (*L*1 and *L*2) and actin core bundle length (*L*3) measurements were performed. (**B**) The loss of Myo6 leads to a significant increase in the mean standard deviation between *L*1 and *L*2 (*sv/+*, 0.017 ± 0.019, $n = 36$ MV vs. *sv/sv*, 0.076 ± 0.039, $n = 36$ MV; $P < 0.00000005$). (**C**) The length of the actin core bundle and length ratio of MV segment/rootlet segment is not affected by the loss of Myo6. The ratio of the total MV core length (*L*3: core within MV plus terminal web rootlet)/(*L*1: the longer MV length/MV) was equivalent (~1.2) in both genotypes; *sv/+* *L*3/*L*1= 1.23 ± 0.1, $n = 40$; *sv/sv* *L*3/*L*1= 1.22 ± 0.05, $n = 40$ MV. Note that measurements were made on a wide range of MV lengths (0.71–1.45 μm) for both genotypes indicating that the ratio of rootlet to MV length is constant regardless of MV length. The assumption is that *L*1 represents MV lengths in *sv/sv* BBs with the least inter-MV membrane perturbation/lifting.

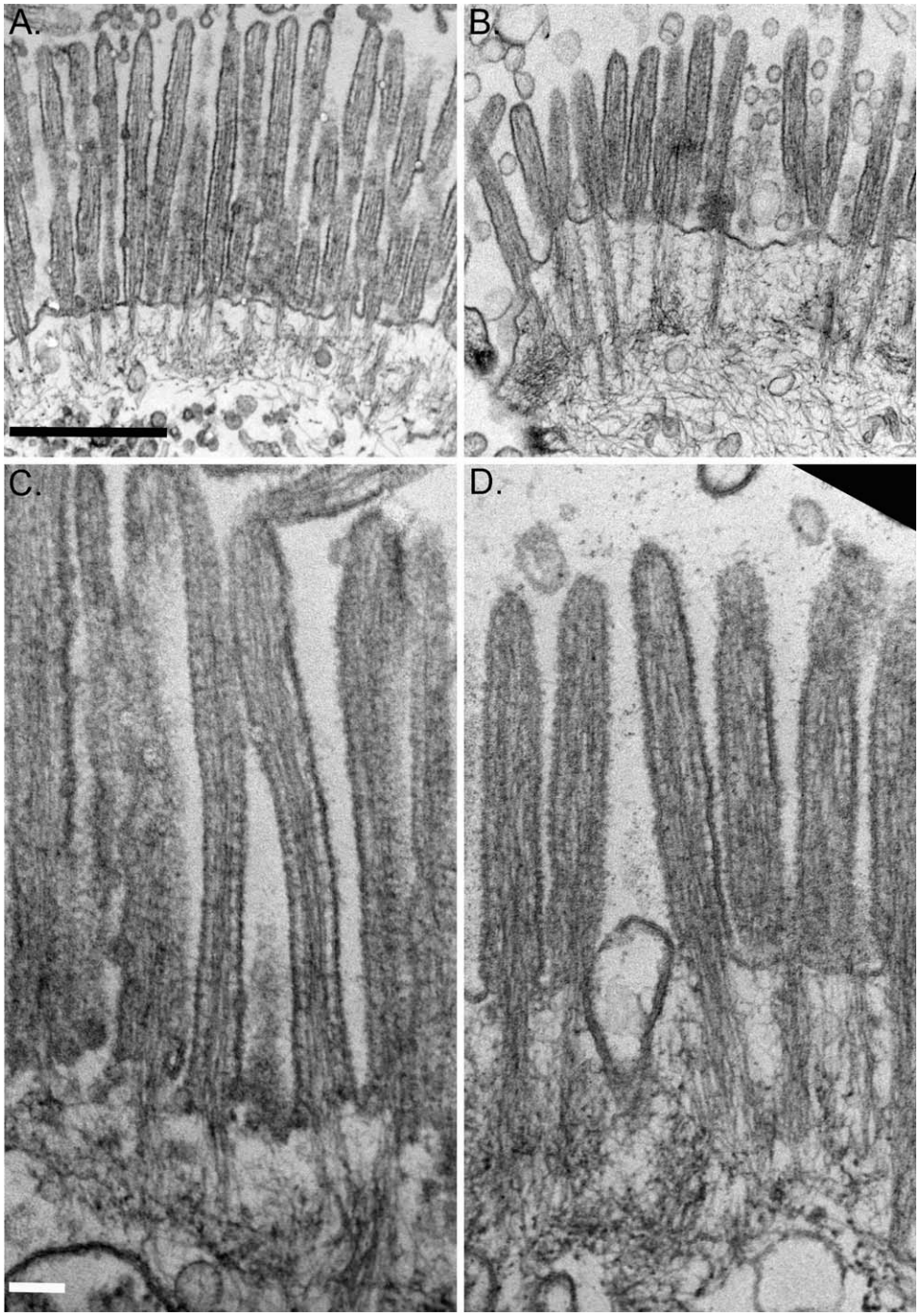

Fig. 4. BB ultrastructure is disrupted by the loss of Myo6. (A) Purified *sv/+* BB examined by TEM. Note that the morphology of inter-MV membrane, actin core bundle, and terminal web are preserved. (**B**) Purified *sv/sv* BB. The inter-MV membrane is completely released from the underlying actin cytoskeleton, causing MV to appear shorter, but the length of the actin core bundle is not affected by the loss of Myo6. There is also an increased amount of intermediate filaments attached to the actin rootlets in the *sv/sv* as compared to *sv/+*. (**C**, **D**) High magnification micrographs of *sv/+* (C) and *sv/sv* (D) MV. In the *sv/+* Myo1a cross bridges are intact and the structure of the actin core bundle is preserved. In *sv/sv* Myo1a cross bridges and actin bundles are preserved, but note the apparent length difference of MV compared to *sv/+* control. The length of the actin core bundle is comparable in both genotypes, suggesting that the apparent length difference is due to lifting of the inter-MV membrane and not due to alteration of the MV actin core. Bar A, B = 500 nm, C, D = 100 nm.

enterocyte, although MV length does vary from short to long along the villus axis. The perturbations of the inter-MV domain in the *sv/sv* results in apparent variations of MV length if length is defined by *L2* (the shorter of the two MV length measurements). Indeed shorter MV lengths in *sv/sv* enterocytes has been previously reported [Ameen and Apodaca, 2007]. However, MV length variations could also result from less precise control of MV

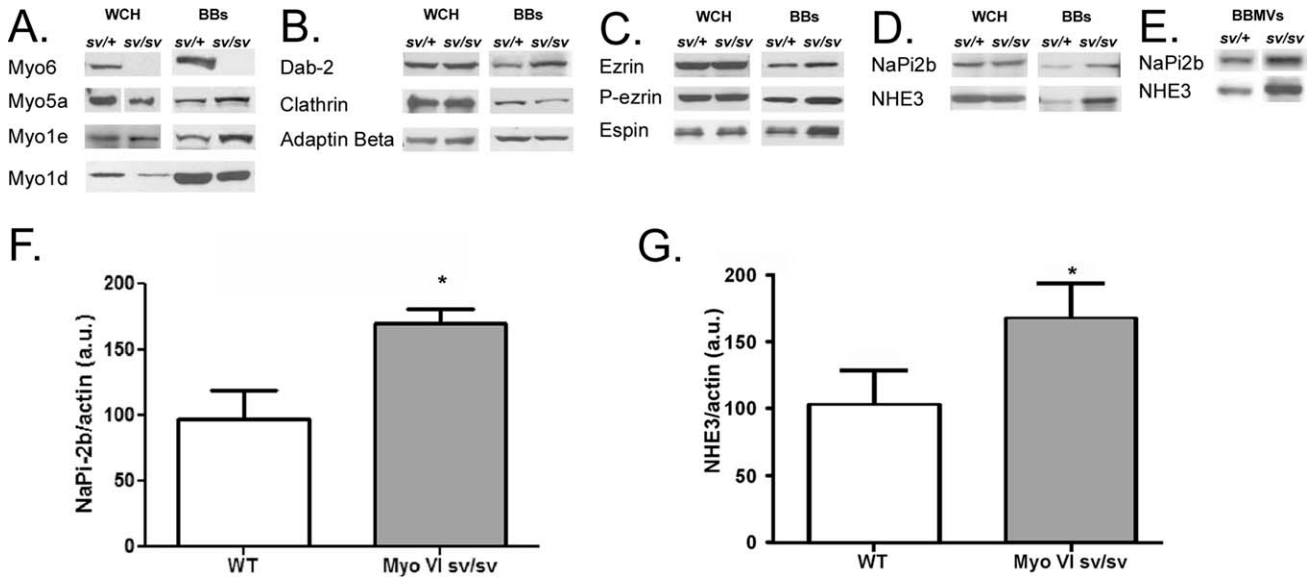

Fig. 5. The loss of Myo6 disrupts protein composition in purified BBs. (Only those proteins which exhibit changes in BB expression are shown; see Table I for a summary of the panel of BB proteins examined, a number of which exhibited no change in expression.) (**A**–**D**) WCH protein levels are generally not affected by the loss of Myo6, with the exception of Myo5a and Myo1d. (A) Other myosins are affected by the loss of Myo6. There is no detectable Myo6 in *sv/sv* BBs; levels of Myo5a and Myo1e are increased in *sv/sv* BBs, and levels of Myo1d are decreased. (B) Endocytic proteins are affected by the loss of Myo6. Levels of Dab-2 are increased, while levels of clathrin and adaptin β are decreased. (C) Actin binding proteins of the MV core are affected by the loss of Myo6. Levels of ezrin, p-ezrin, and espin are all increased in *sv/sv* BBs. (D) Levels of NaPi2b and NHE3 are both increased in *sv/sv* BBs. (**E**–**G**) Levels of NaPi2b and NHE3 are both increased in purified *sv/sv* BBMVs. Purified BBMVs are significantly ($P < 0.005$) enriched for both NaPi2b and NHE3, showing that the increased levels of these two proteins are due to association with the BB plasma membrane, and not with the subapical endosomal compartment. Both NaPi2b and NHE3 show a ∼1.6× increase in *sv/sv* as compared to WT. a.u., arbitrary units.

actin core length. To distinguish between these two possibilities, the ratio of total MV core length (*L*3 in Fig. 3A) to *L*1 (the longest of the MV base to MV tip measurements/MV) was determined. This assumes that *L*1 represents MV lengths with minimal shortening due to inter-MV perturbation and thus are comparable to that seen in control enterocytes. In both *sv/+* and *sv/sv*, the ratio of MV core length to MV length was ∼1.2. These ratios were determined using measurements from a wide range of MV lengths. This indicates that the ratio of the MV segment of the core/rootlet segment is constant independent of MV length (Fig. 3C). These results suggest that the loss of Myo6 affects inter-MV membrane tethering to the MV core but in contrast to the Myo1a KO [Tyska et al., 2005], not assembly and length control of the underlying actin core.

The apparent detachment of the BB membrane from the MV core within the inter-MV domain in *sv/sv* enterocytes is enhanced in isolated BBs. Normal looking BBs are observed in the *sv/+* control (Fig. 4A); however, much of the BB membrane has lifted off of the inter-MV region in the *sv/sv* mouse (Fig. 4B). This increased lifting is likely due to the breaking of junctional complexes during the preparation, eliminating tethering at the lateral margins in the sub-apical region of the enterocyte. Myo1a cross bridges between the MV actin core and BB membrane are present in both *sv/+* and *sv/sv* (Figs. 4C and 4D) and presumably prevent complete detachment of the BB membrane from the underlying actin cytoskeleton. One puzzling observation is that Myo1a bridges are not present on the regions of MV core from which the membrane linkages have been lost. As noted below, there is no change in levels of Myo1a, even though there are significantly fewer Myo1a-membrane bridges. One possible explanation is that the Myo1a remains bound to the BB membrane or that the spiral order of the Myo1a bridges is disordered upon membrane detachment. However, this is not the case when the BB membrane is removed with detergent [Mooseker and Tilney, 1975].

The Molecular Composition of the BB Membrane and Cytoskeleton is Altered in *sv/sv* Enterocytes

Immunoblot analysis of isolated BBs revealed several changes in protein composition between *sv/+* and *sv/sv* mice. WCHs were analyzed for total protein levels and (with the exception of Myo1d and MyoVa, in which there is less total protein in the *sv/sv*) no significant differences were observed, suggesting that the BB compositional defects observed are due to altered subcellular localization or affinity for the BB during isolation, and not changes in

Table I. Summary of Compositional Changes in *sv/sv* BBs

Region/component	Change relative to *sv/+*
BB membrane	
Sucrase isomaltase	n.c.
Galectin-4	n.c.
Alkaline phosphatase	n.c.
MV core	
Myo1a	n.c.
Myo1c	n.c.
Myo1d	↓
Villin	n.c.
Fimbrin	n.c.
Ezrin	↑
P-ezrin	↑
Espin	↑
Intermicrovillar/terminal web	
Myo6	Absent
Clathrin	↓
Adaptin β	↓
Dab-2	↑
Myo1e	↑
Myo2a	n.c.
Myo5a	↑
Spectrin	n.c.
Membrane transporters	
NaPi2b	↑
NHE3	↑

n.c., no change; ↑/↓, increase/decrease in level.

levels of protein expression (Fig. 5). As expected there is no detectable Myo6 in the *sv/sv* mutant, while Myo5a and Myo1e levels are both increased, and Myo1d levels are decreased in the absence of Myo6 (Fig. 5A). Four proteins that are involved with clathrin mediated endocytosis showed altered levels in the *sv/sv* BB (Fig. 5B). There were slight but reproducible reductions in clathrin and adaptin β levels reduced compared to *sv/+*, in contrast Myo1e and Dab-2 levels were increased in the *sv/sv* mouse. The Dab-2 observations are consistent with the localization results of Collaco et al. [2010]. The levels of the MV core actin binding proteins, ezrin, phosphorylated-ezrin (p-ezrin), the active form of this actin-membrane linker protein [Fievet et al., 2004] and the MV actin filament bundling protein espin were all increased in the *sv/sv* BB (Fig. 5C). There are also increased levels of NHE3 and NaPi2b in the *sv/sv* BB as compared to *sv/+* (Fig. 5D). Both NHE3 and NaPi2b have been shown to exhibit regulated trafficking between the BB membrane and apical endosomal compartment (for reviews of NHE3 and NaPi2b regulation see Giral et al. [2009]; He and Yun [2010]). For both NHE3 and NaPi2b, we verified that the increased BB association was due to increased BB membrane content and not copurifying subapical endosomal membranes by immunoblot analysis of isolated BBMVs (Fig. 5E) prepared by Mg^{2+} precipitation. Quantification of BBMV immunoblots showed that levels of both NaPi2b and NHE3 were significantly increased in *sv/sv* as compared to *sv/+* (Figs. 5F and 5G). There was a 1.6× increase in the amount of both NaPi2b and NHE3 in *sv/sv* BBMVs as compared with WT control. Unlike isolated BBs that can contain terminal web-associated subapical vesicles and lateral junctional membrane, the BBMV preparations consists of MV core containing vesicles derived solely from the MV/BB membrane. These results suggest that, as has been shown previously for CFTR [Ameen and Apodaca, 2007], trafficking of these proteins from the BB membrane to the endosome is a Myo6-dependent process. These compositional changes, as well as several other BB components that are not affected by the loss of Myo6 are summarized in Table I.

Immunofluorescence microscopy of mouse intestine was used to further analyze the compositional changes that were observed by immunoblot of purified BBs. For example, the staining intensity (but not localization) of the actin binding proteins espin (Fig. 6A) and p-ezrin (Fig. 6B) in the BB domain of the *sv/sv* enterocyte is significantly greater than that seen in the sv/+ control. Also consistent with the biochemical analyses, the intensity of clathrin staining within the inter-MV domain is reduced in the *sv/sv* enterocyte, although levels of perinuclear clathrin staining are comparable in *sv/sv* and *sv/+* enterocytes (Fig. 7A). The loss of Myo6 leads to the recruitment of another myosin which as noted above is involved with endocytosis, Myo1e [Krendel et al., 2007] (Fig. 7B). In contrast, although levels of Myo5a are increased when assayed by immunoblot of isolated BBs, there was not an obvious recruitment of Myo5a to the BB domain when examined by immunofluorescence microscopy (data not shown), suggesting that the differences seen are due to increased affinity and retention during BB purification.

Myo6 is Involved with Clathrin-Mediated Endocytosis of Lactoferrin

The iron carrying protein lactoferrin was used as a marker to determine if the loss of Myo6 has an effect on clathrin-mediated endocytosis in the mouse small intestine. Explants of pig small intestine have been shown to bind lactoferrin to the apical BB of enterocytes, and within 30 min discrete, internalized puncta can be seen [Nielsen et al., 2010]. In the mouse small intestine, lactoferrin has been shown to use the mouse homologue of the human lactoferrin receptor intelectin as its receptor [Suzuki and Lonnerdal, 2004]. In our studies we used cultured

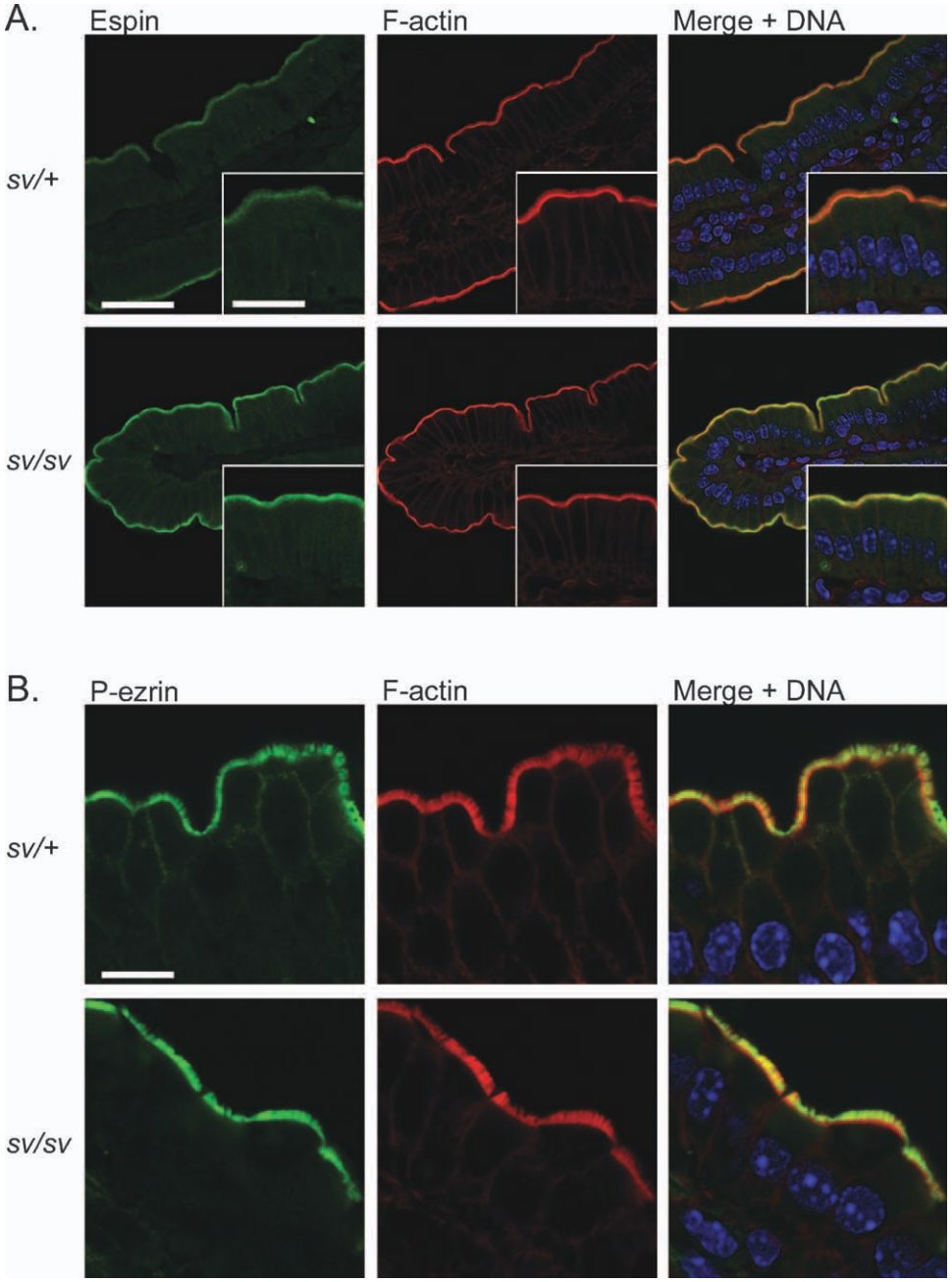

Fig. 6. The loss of Myo6 affects actin binding protein levels in the BB. (**A**) Immunolocalization of espin shows that protein localization is not affected by the loss of Myo6, but the level of espin is increased in the *sv/sv* duodenum as compared to *sv/+*. (**B**) *Sv/+* control and *sv/sv* duodenum stained with p-ezrin antibody. Note that localization of p-ezrin is not affected by the loss of Myo6, but the relative intensity level of p-ezrin staining is also increased in the *sv/sv* BB. Bar A = 35 μm, inset = 20 μm, B = 10 μm.

explants of jejunum to monitor endocytosis of lactoferrin, with experiments being done at both 4°C and 37°C. At 4°C lactoferrin appears to bind to BB membrane equally in both *sv/+* and *sv/sv*, suggesting that the loss of Myo6 does not affect the localization of the lactoferrin receptor intelectin (Fig. 8A). There was no internalization of lactoferrin observed at 4°C in either genotype. When explants were cultured at 37°C lactoferrin was internalized in the *sv/+* jejunum explants, but in the *sv/sv* there was no internalization of lactoferrin (Fig. 8B). All of the detectable lactoferrin was still bound to the MV membrane. Based on previous studies that showed high expression levels of lactoferrin receptor in the 10-day-old neonate mouse small intestine [Lopez et al., 2006], we stained 10-day-old *sv/+* and *sv/sv* small intestine cryosections for endogenous lactoferrin and discovered that both genotypes had comparable levels of internalized lactoferrin (Fig. 9), suggesting a mechanism of uptake that is not dependent on Myo6 in the neonatal mouse.

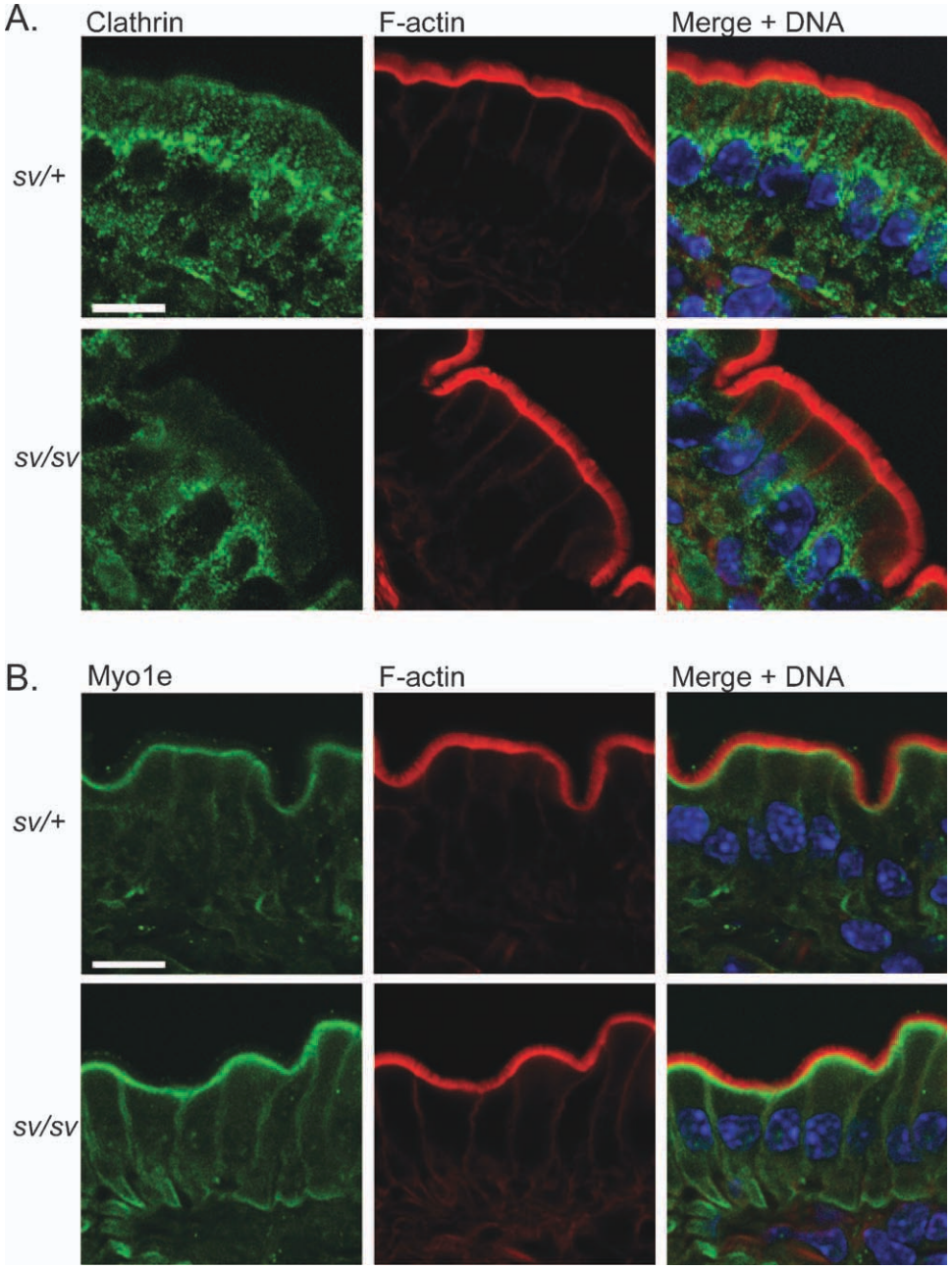

Fig. 7. The loss of Myo6 affects the localization of BB endocytic proteins. (**A**) Immunostaining of *sv*/+ jejunum shows that clathrin is localized to the subapical and perinuclear regions of the enterocyte. Staining of clathrin in the *sv/sv* jejunum shows that the majority of the subapical clathrin staining is lost, and the majority of the protein is localized to the perinuclear region of the cell. (**B**) The loss of Myo6 leads to the recruitment of additional Myo1e to the subapical region of the *sv/sv* duodenum. Staining intensity levels of subapical Myo1e are greatly increased in the *sv/sv* as compared to *sv*/+ control. Bar = 10 μm.

Myo6 is Required for Trafficking of NHE3 and NaPi2b from the BB Membrane to the Subapical Endosome

As noted above, there are elevated levels of both NHE3 and NaPi2b in isolated *sv/sv* BBs and BBMVs. Consistent with these results NHE3 is localized to both the BB membrane and the subapical, presumably endosomal domain in both in both the *sv*/+ and *sv/sv* mouse (Fig. 10). However, the intensity of BB staining is greater in the *sv/sv* enterocyte. Since total cell expression levels of NHE3 are the same in *sv/sv* and *sv*/+, these results indicate that there is likely to be reduced recycling to the subapical endosomal domain in the *sv/sv* enterocyte. Similar results were obtained for localization of NaPi2b in mice fed on high and low Pi diets. Previous studies in the rat have shown that low Pi diet (0.1%) causes NaPi2b to move out to the BB membrane in order to maximize uptake of Pi, while a high Pi diet (1.2%) causes NaPi2b to be internalized to an apical endosomal compartment in order to reduce uptake of dietary Pi [Giral et al., 2009]. After

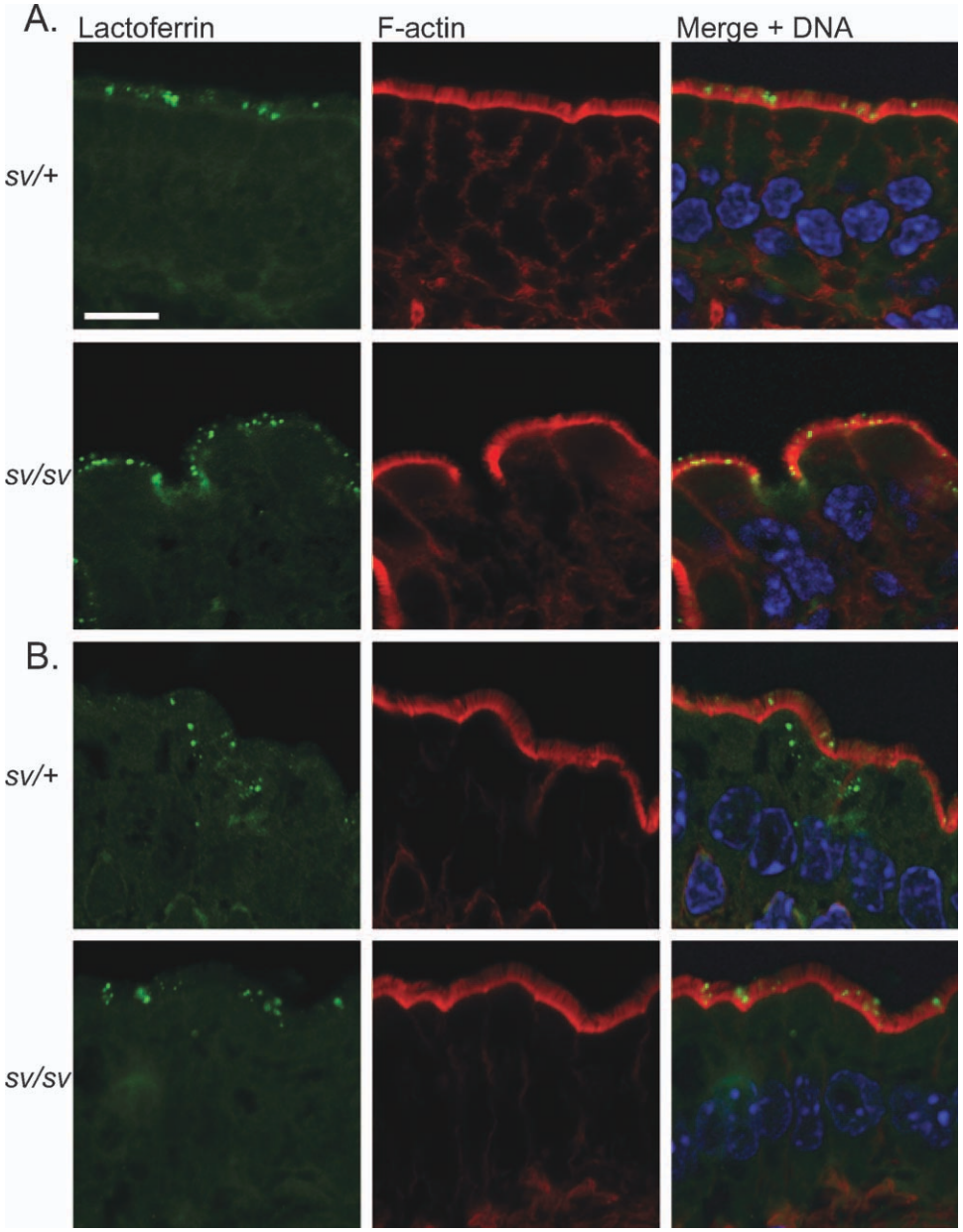

Fig. 8. The loss of Myo6 inhibits endocytosis of lactoferrin in jejunum explants. (**A**) *sv*/+ and *sv/sv* jejunum explants cultured for 30 min at 4°C in the presence of lactoferrin. Note that lactoferrin is surface bound in both genotypes, and there is no internalization. (**B**) *sv*/+ and *sv/sv* jejunum explants cultured for 30 min at 37°C in the presence of lactoferrin. Internalized puncta are clearly seen in the *sv*/+ control, while there is no uptake of lactoferrin in the *sv/sv* mutant. Bar = 10 μm.

feeding a low Pi diet to *sv*/+ and *sv/sv* mice for two weeks we saw NaPi2b localization in the BB membrane of distal ileum enterocytes in both genotypes. There was no difference between the two genotypes, suggesting that Myo6 is not essential for movement to/retention of NaPi2b in the BB membrane (Fig. 11A). After feeding high Pi food to *sv*/+ mice for 2 weeks it was observed that NaPi2b was absent from the BB membrane and restricted in localization to the subapical domain (Fig. 11B). In contrast there was marked retention of NaPi2b in the BB membrane of the *sv/sv* enterocyte in addition to subapical localization; this result indicates that Myo6 is required to regulate the cellular distribution of NaPi2b in response to the amount of Pi present in the diet. Standard lab diet yielded results identical to the high Pi diet (data not shown).

Discussion

The loss of Myo6 function has numerous and functionally diverse consequences in the *sv/sv* enterocyte. These include effects consistent with defects observed in other cell types expressing Myo6 including defects in apical membrane tethering to the underlying actin cytoskeleton, defects in endocytic membrane trafficking, and altered expression of

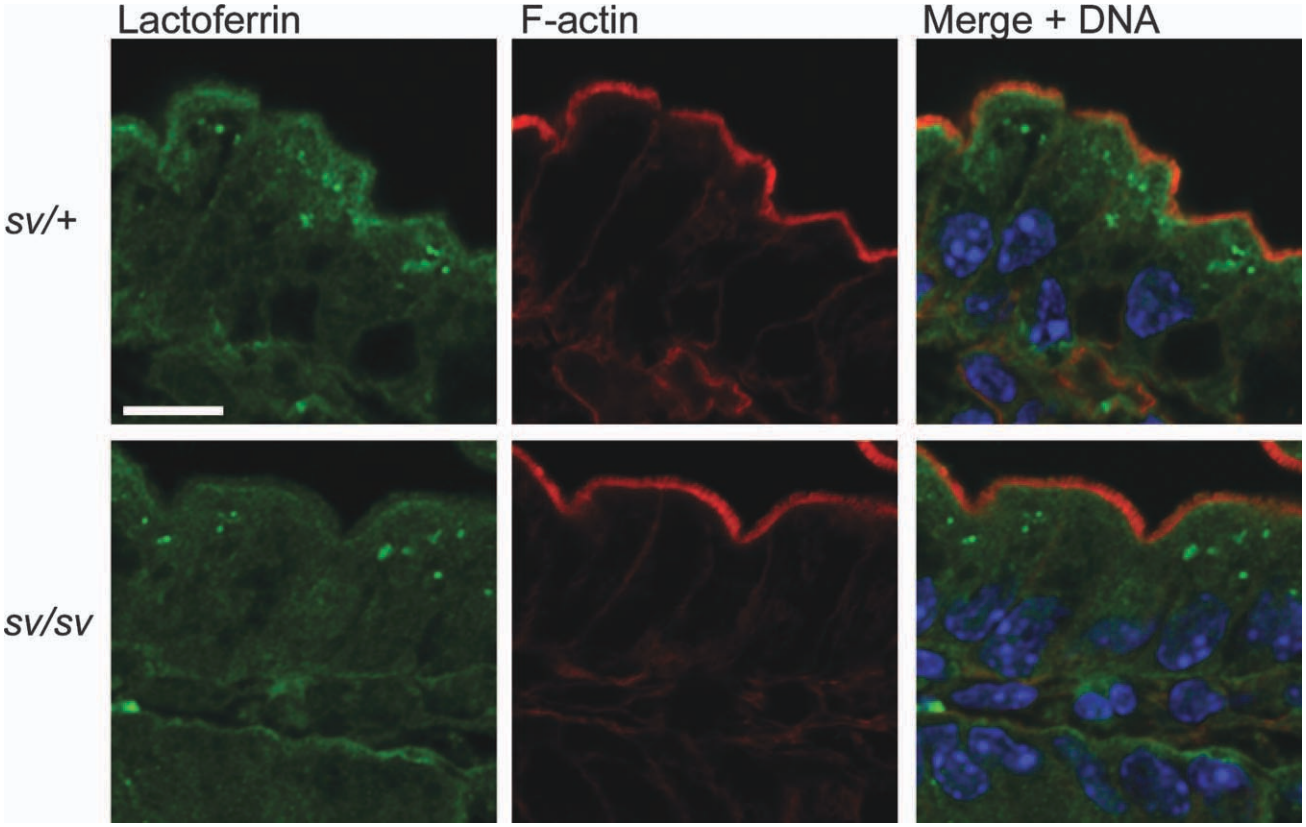

Fig. 9. Neonatal mice can internalize lactoferrin in the absence of Myo6. Ten-day-old jejunum from nursing pups was processed for microscopy as described in Materials and Methods and endogenous lactoferrin was visualized by immunofluorescence microscopy. Similar amounts of internalized lactoferrin can be seen in both genotypes, suggesting that the neonatal mouse uses a Myo6-independent pathway for endocytosis of lactoferrin, in contrast to the adult mouse, which cannot internalize lactoferrin in the absence of Myo6. Bar = 10 μm.

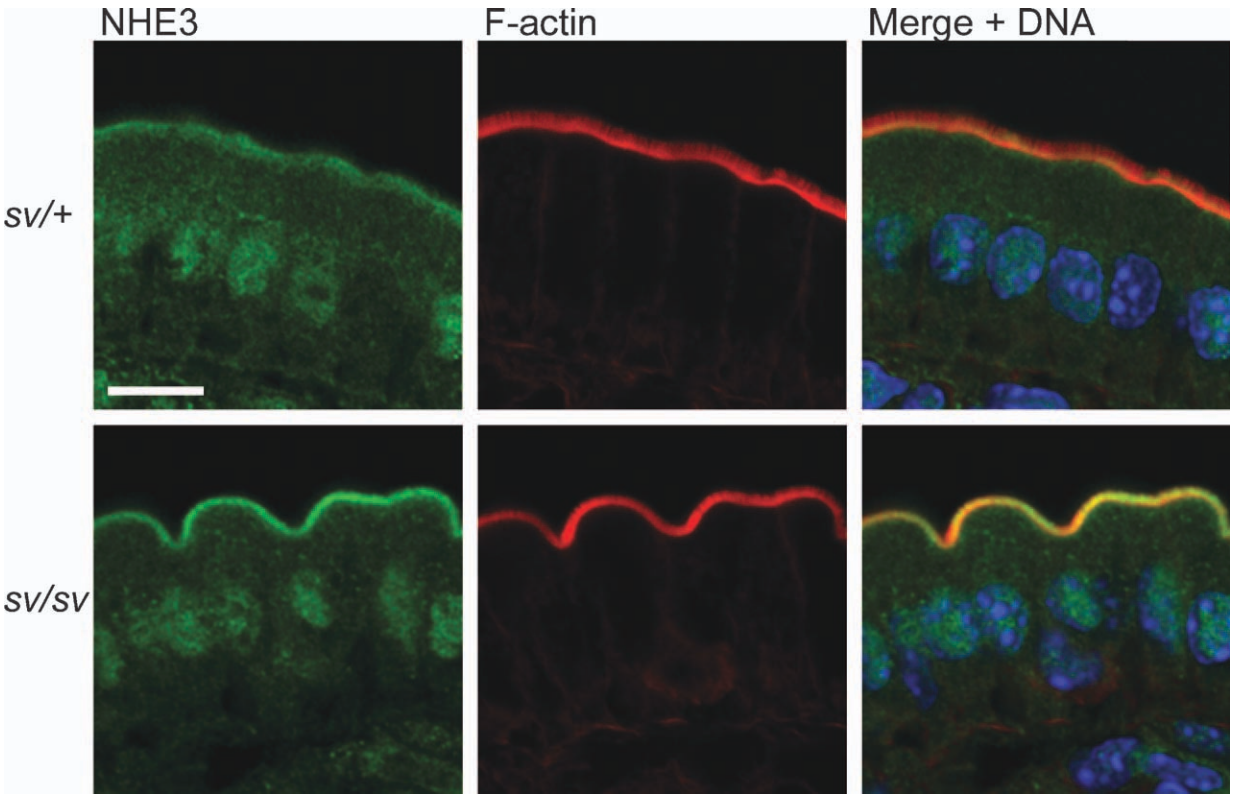

Fig. 10. NHE3 is retained in the *sv/sv* BB membrane. The staining intensity of NHE3 is greater in the BB membrane of the *sv/sv* jejunum, as compared to as *sv*/+, suggesting that Myo6 is needed for proper regulation of cell surface levels of NHE3. Bar = 10 μm.

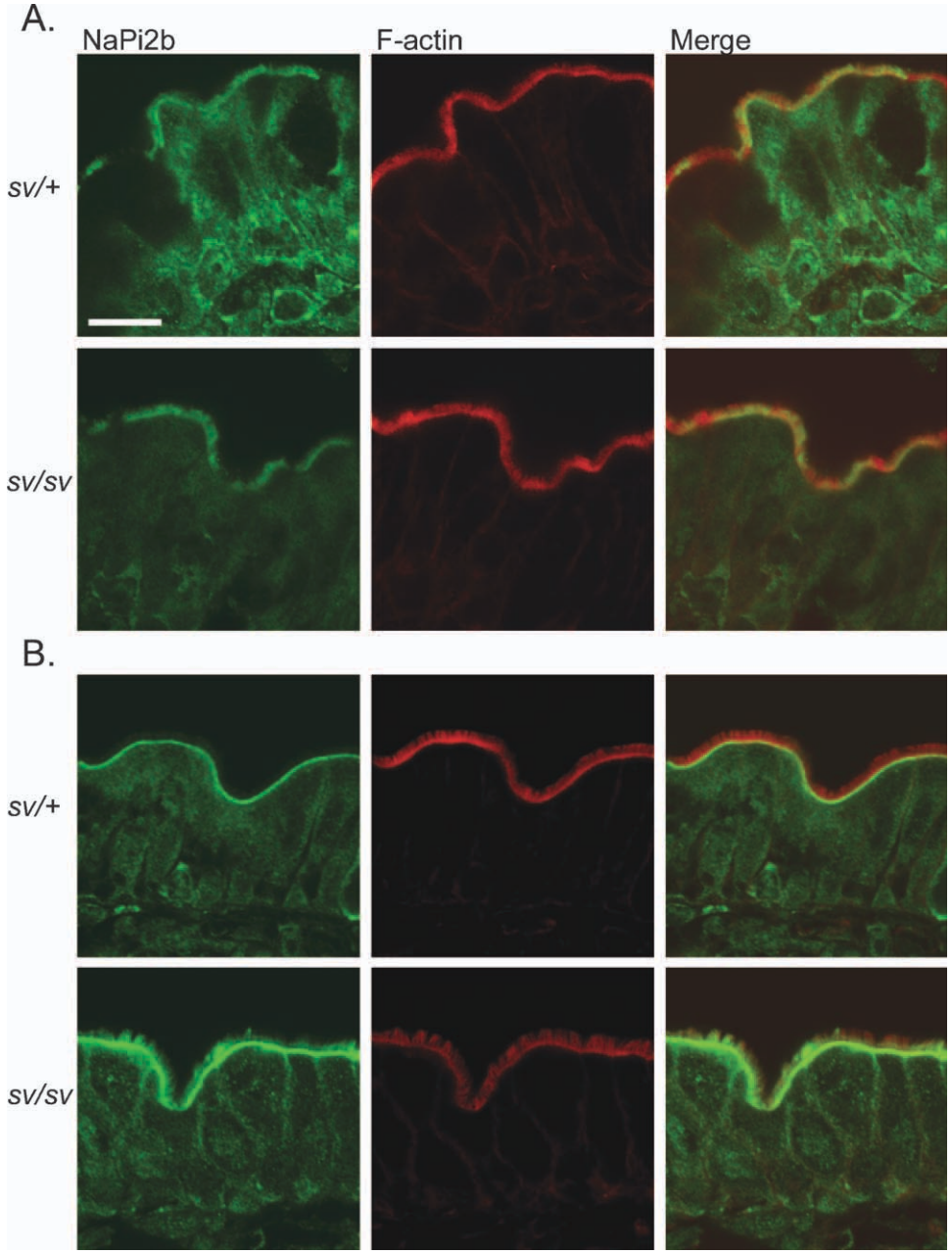

Fig. 11. NaPi2b trafficking is disrupted by the loss of Myo6 under conditions of high dietary Pi. (**A**) *Sv/+* and *sv/sv* distal ileum under low dietary Pi conditions. Notice that apical NaPi2b localization is in the MV, presumably to maximize uptake of dietary Pi. Localization is similar in both genotypes, implying that Myo6 is not a critical component in the delivery of NaPi2b to the BB membrane. (**B**) *Sv/+* and *sv/sv* distal ileum under high dietary Pi conditions. Nearly all of the NaPi2b in the *sv/+* has been internalized, while a large amount is still present in the BB membrane of the *sv/sv* mouse. This result suggests a direct role for Myo6 in the internalization of NaPi2b in response to elevated levels of dietary Pi. Bar = 10 μm.

components of the BB-associated clathrin-mediated endocytic machinery with which Myo6 is known to associate. The numerous compositional changes in components of the BB actin cytoskeleton including increases or decreases in BB association of several myosins, and increased association of components of the MV actin core are novel and as discussed below, suggest functional synergies between the sole minus-end directed motor of the BB cytoskeleton and other BB components with no obvious structural and/or functional overlap. An unexpected outcome of these studies is that there is very little overlap between these defects and the array of structural and compositional defects observed in the Myo1a KO even though one of the most striking effects of loss of Myo1a is the loss of Myo6 from the inter-MV domain [Tyska et al., 2005].

The ultrastructural studies presented here demonstrate that Myo6, which is localized to the inter-MV domain, is required for proper tethering of the BB membrane at the

bases of MV. These perturbations of the inter-MV domain could result from either detachment of the BB membrane from the underlying MV core or the failure to form such attachments during BB assembly. This inter-MV perturbation that can result in MV fusion is analogous to that seen in the stereocilia of the *sv/sv* hair cell. However, the Myo6-dependent tethering function is not unique to all epithelial cells that express subapical Myo6, since no basal lifting of the BB membrane is observed in the *sv/sv* kidney proximal tubule epithelial cell [Gotoh et al., 2010]. It is interesting to note that this apparent lifting of the membrane may be dependent on the plus-end directed force exerted on the BB membrane by the major plus-end motor associated with the BB membrane, Myo1a. This is because no such membrane lifting and MV fusion is observed in the Myo1a KO BB even though Myo6 is lost from the BB. Instead detachment of the BB membrane from the actin core at the tips of MV is observed [Tyska et al., 2005]. Although the lifting of the BB membrane at the base of MV results in shorter MV in the *sv/sv* enterocyte (as defined by the length of the MV from base to tip), as noted previously [Ameen and Apodaca, 2007], the loss of Myo6 has no obvious effects on the overall length of the MV actin core (Fig. 3). This is in contrast to the loss of precise MV actin core filament length control in the Myo1a KO [Tyska et al., 2005]. Thus, the molecular basis for how the enterocyte controls MV actin filament length is dependent in part on Myo1a, perhaps through controlling plus-end tension on the MV membrane, and not on Myo6.

Except for the decreases in clathrin and adaptin β, and the previously observed increased BB association of Dab2 [Collaco et al., 2010], other compositional alterations observed were unexpected as there are no obvious functional, and in some instances subcellular localization overlaps between the proteins observed to have altered BB expression. Two components whose association with the BB cytoskeleton is increased in the *sv/sv* enterocyte, Myo5a [Heintzelman et al., 1994] and Myo1e [Skowron et al., 1998] are also localized to the subapical terminal web domain of the BB. As noted above, the increase in Myo5a content in the isolated BB may be due to changes in retention during isolation since increased immunostaining intensity was not observed. The increase in inter-MV Myo1e as assessed both by content in isolated BBs and by immunolocalization was unexpected, since Myo1e is essentially lost from the BB in the Myo1a KO, in which Myo6 is also absent (but expressed at WT levels in the cell). Myo1e has also been implicated in clathrin-mediated endocytosis through its association with synaptojanin and dynamin [Krendel et al., 2007]. Perhaps in the total absence of Myo6 (as compared to the Myo1a KO) there is less competition for binding partners with which Myo1e and Myo6 either directly or indirectly interact, resulting in increased BB associated Myo1e. This change in competition for binding partners may also allow Myo1e to assume a partial role in membrane tethering in the absence of Myo6. The reduced total cell levels of Myo1d was unexpected in that in general in both *sv/sv* and Myo1a KO, most proteins we have assessed no not exhibit changes in expression levels. Myo1d is located at both the base and tips of MV [Benesh et al., 2010]. Perhaps the inter-MV perturbations seen in the *sv/sv* BB destabilizes its association with the BB.

Both total ezrin, and p-ezrin are increased in the *sv/sv* BB cytoskeleton based both on biochemical analysis of isolated BBs and in situ localization. Previous studies using an ezrin KO mouse [Saotome et al., 2004] show that the BB ultrastructural defects in the absence of ezrin are very similar, if not more severe, to those seen due to the loss of Myo6 that we have described in this study. Since p-ezrin is the active form of ezrin, which in its unfolded state can bind both the BB membrane and the actin core, this increase may be a compensatory response to the loss of Myo6 mediated tension. If so, it is quite puzzling why no change in ezrin expression is seen in the Myo1a KO, where Myo1a, which plays a key role in membrane tethering [Nambiar et al., 2009], is absent and Myo6 is reduced. The increase in the MV actin core bundling protein espin is also a puzzle. Espin, together with villin and fimbrin (I plastin, plastin 1) crosslink MV actin filaments along the length of the MV actin core. Perhaps the loss of Myo6 mediated minus-end tension on the MV core alters the helical structure of filaments with which it interacts, increasing the binding affinity of espin for actin, or the loss of Myo6 from the inter MV region may also destabilize the rootlet region of the MV actin bundle, causing espin to be recruited in order to stabilize the MV actin bundle.

As summarized in the Introduction, Myo6 has been implicated in clathrin-mediated endocytosis in numerous cell types and in the internalization of many different cargo molecules. However, as noted above, not all cargos require Myo6 for internalization. Presumably this is because the clathrin adaptor molecules with which Myo6 interacts such as Dab2 and GIPC are cargo selective. In the case of the cargo molecule lactoferrin, we show that the role of Myo6 is developmentally regulated, since uptake is normal in the *sv/sv* neonate and impaired in the adult. This could be due to differences in the receptors involved (e.g., lipid raft vs. nonraft associated) and/or expression of clathrin adaptors. In contrast, the results presented here show that Myo6 is involved in the regulated BB membrane ↔ endosome trafficking of three membrane proteins under very different modes of physiologic regulation, CFTR [Ameen and Apodaca, 2007], NHE3, and NaPi2b. Indeed, CFTR and NHE3 respond in opposite directions to the same stimuli; cAMP stimulates the exocytosis of CFTR [Barrett and Keely, 2000] while it induces internalization of NHE3 [Donowitz and

Li, 2007]. The involvement of Myo6 in the trafficking of such a diverse array of membrane proteins in a single cell type suggests it may play a central and ubiquitous role in physiologically regulated trafficking of membrane components at least in the enterocyte and a selective role in cargo dependent and constitutive clathrin mediated endocytosis.

Acknowledgments

This work was supported by NIH grants GM 073823 DK-25387, DK 25387 to M. Mooseker and NIH DK 066029 to M. Levi. We also thank Dr. James Bartles for the espin antibody used in this study.

References

Ameen N, Apodaca G. 2007. Defective CFTR apical endocytosis and enterocyte brush border in myosin VI-deficient mice. Traffic 8(8):998–1006.

Avraham KB, Hasson T, Steel KP, Kingsley DM, Russell LB, Mooseker MS, Copeland NG, Jenkins NA. 1995. The mouse Snell's waltzer deafness gene encodes an unconventional myosin required for structural integrity of inner ear hair cells. Nat Genet 11(4):369–375.

Barrett KE, Keely SJ. 2000. Chloride secretion by the intestinal epithelium: molecular basis and regulatory aspects. Annu Rev Physiol 62:535–572.

Bartles JR, Wierda A, Zheng L. 1996. Identification and characterization of espin, an actin-binding protein localized to the F-actin-rich junctional plaques of Sertoli cell ectoplasmic specializations. J Cell Sci 109(Pt 6):1229–1239.

Benesh AE, Nambiar R, McConnell RE, Mao S, Tabb DL, Tyska MJ. 2010. Differential localization and dynamics of class I myosins in the enterocyte microvillus. Mol Biol Cell 21(6):970–978.

Biemesderfer D, Mentone SA, Mooseker M, Hasson T. 2002. Expression of myosin VI within the early endocytic pathway in adult and developing proximal tubules. Am J Physiol Renal Physiol 282(5):F785–F794.

Buss F, Kendrick-Jones J. 2008. How are the cellular functions of myosin VI regulated within the cell? Biochem Biophys Res Commun 369(1):165–175.

Buss F, Kendrick-Jones J. 2011. Multifunctional myosin VI has a multitude of cargoes. Proc Natl Acad Sci USA 108(15):5927–5928.

Chibalina MV, Puri C, Kendrick-Jones J, Buss F. 2009. Potential roles of myosin VI in cell motility. Biochem Soc Trans 37(Pt 5): 966–970.

Collaco A, Jakab R, Hegan P, Mooseker M, Ameen N. 2010. Alpha-AP-2 directs myosin VI-dependent endocytosis of cystic fibrosis transmembrane conductance regulator chloride channels in the intestine. J Biol Chem 285(22):17177–17187.

Deol MS, Green MC. 1966. Snell's waltzer, a new mutation affecting behaviour and the inner ear in the mouse. Genet Res 8(3): 339–345.

Donowitz M, Li X. 2007. Regulatory binding partners and complexes of NHE3. Physiol Rev 87(3):825–872.

Espreafico EM, Cheney RE, Matteoli M, Nascimento AA, De Camilli PV, Larson RE, Mooseker MS. 1992. Primary structure and cellular localization of chicken brain myosin-V (p190), an unconventional myosin with calmodulin light chains. J Cell Biol 119(6):1541–1557.

Fievet BT, Gautreau A, Roy C, Del Maestro L, Mangeat P, Louvard D, Arpin M. 2004. Phosphoinositide binding and phosphorylation act sequentially in the activation mechanism of ezrin. J Cell Biol 164(5):653–659.

Giral H, Caldas Y, Sutherland E, Wilson P, Breusegem S, Barry N, Blaine J, Jiang T, Wang XX, Levi M. 2009. Regulation of rat intestinal Na-dependent phosphate transporters by dietary phosphate. Am J Physiol Renal Physiol 297(5):F1466–F1475.

Gotoh N, Yan Q, Du Z, Biemesderfer D, Kashgarian M, Mooseker MS, Wang T. 2010. Altered renal proximal tubular endocytosis and histology in mice lacking myosin-VI. Cytoskeleton (Hoboken) 67(3):178–192.

Hasson T, Mooseker MS. 1994. Porcine myosin-VI: characterization of a new mammalian unconventional myosin. J Cell Biol 127(2): 425–440.

Hasson T, Gillespie PG, Garcia JA, MacDonald RB, Zhao Y, Yee AG, Mooseker MS, Corey DP. 1997. Unconventional myosins in inner-ear sensory epithelia. J Cell Biol 137(6):1287–1307.

He P, Yun CC. 2010. Mechanisms of the regulation of the intestinal Na+/H+ exchanger NHE3. J Biomed Biotechnol 2010:238080.

Heintzelman MB, Hasson T, Mooseker MS. 1994. Multiple unconventional myosin domains of the intestinal brush border cytoskeleton. J Cell Sci 107(Pt 12):3535–3543.

Holt JP, Bottomly K, Mooseker MS. 2007. Assessment of myosin II, Va, VI and VIIa loss of function on endocytosis and endocytic vesicle motility in bone marrow-derived dendritic cells. Cell Motil Cytoskeleton 64(10):756–766.

Inoue A, Saito J, Ikebe R, Ikebe M. 2002. Myosin IXb is a single-headed minus-end-directed processive motor. Nat Cell Biol 4(4): 302–306.

Krendel M, Osterweil EK, Mooseker MS. 2007. Myosin 1E interacts with synaptojanin-1 and dynamin and is involved in endocytosis. FEBS Lett 581(4):644–650.

Liao W, Elfrink K, Bahler M. 2010. Head of myosin IX binds calmodulin and moves processively toward the plus-end of actin filaments. J Biol Chem 285(32):24933–24942.

Lopez V, Suzuki YA, Lonnerdal B. 2006. Ontogenic changes in lactoferrin receptor and DMT1 in mouse small intestine: implications for iron absorption during early life. Biochem Cell Biol 84(3):337–344.

Mooseker MS, Tilney LG. 1975. Organization of an actin filament-membrane complex. Filament polarity and membrane attachment in the microvilli of intestinal epithelial cells. J Cell Biol 67(3): 725–743.

Mooseker MS, Pollard TD, Fujiwara K. 1978. Characterization and localization of myosin in the brush border of intestinal epithelial cells. J Cell Biol 79(2 Pt 1):444–453.

Nambiar R, McConnell RE, Tyska MJ. 2009. Control of cell membrane tension by myosin-I. Proc Natl Acad Sci USA 106(29): 11972–11977.

Nielsen SM, Hansen GH, Danielsen EM. 2010. Lactoferrin targets T cells in the small intestine. J Gastroenterol 45(11):1121–1128.

O'Connell CB, Mooseker MS. 2003. Native Myosin-IXb is a plus-, not a minus-end-directed motor. Nat Cell Biol 5(2):171–172.

O'Connell CB, Tyska MJ, Mooseker MS. 2007. Myosin at work: motor adaptations for a variety of cellular functions. Biochim Biophys Acta 1773(5):615–630.

Osterweil E, Wells DG, Mooseker MS. 2005. A role for myosin VI in postsynaptic structure and glutamate receptor endocytosis. J Cell Biol 168(2):329–338.

Roux I, Hosie S, Johnson SL, Bahloul A, Cayet N, Nouaille S, Kros CJ, Petit C, Safieddine S. 2009. Myosin VI is required for the

proper maturation and function of inner hair cell ribbon synapses. Hum Mol Genet 18(23):4615–4628.

Saotome I, Curto M, McClatchey AI. 2004. Ezrin is essential for epithelial organization and villus morphogenesis in the developing intestine. Dev Cell 6(6):855–864.

Self T, Sobe T, Copeland NG, Jenkins NA, Avraham KB, Steel KP. 1999. Role of myosin VI in the differentiation of cochlear hair cells. Dev Biol 214(2):331–341.

Skowron JF, Bement WM, Mooseker MS. 1998. Human brush border myosin-I and myosin-Ic expression in human intestine and Caco-2BBe cells. Cell Motil Cytoskeleton 41(4):308–324.

Suzuki YA, Lonnerdal B. 2004. Baculovirus expression of mouse lactoferrin receptor and tissue distribution in the mouse. Biometals 17(3):301–309.

Swiatecka-Urban A, Boyd C, Coutermarsh B, Karlson KH, Barnaby R, Aschenbrenner L, Langford GM, Hasson T, Stanton BA. 2004. Myosin VI regulates endocytosis of the cystic fibrosis transmembrane conductance regulator. J Biol Chem 279(36):38025–38031.

Tyska MJ, Mackey AT, Huang JD, Copeland NG, Jenkins NA, Mooseker MS. 2005. Myosin-1a is critical for normal brush border structure and composition. Mol Biol Cell 16(5):2443–2457.

Warner CL, Stewart A, Luzio JP, Steel KP, Libby RT, Kendrick-Jones J, Buss F. 2003. Loss of myosin VI reduces secretion and the size of the Golgi in fibroblasts from Snell's waltzer mice. EMBO J 22(3):569–579.

Wells AL, Lin AW, Chen LQ, Safer D, Cain SM, Hasson T, Carragher BO, Milligan RA, Sweeney HL. 1999. Myosin VI is an actin-based motor that moves backwards. Nature 401(6752):505–508.

Yang LE, Maunsbach AB, Leong PK, McDonough AA. 2005. Redistribution of myosin VI from top to base of proximal tubule microvilli during acute hypertension. J Am Soc Nephrol 16(10): 2890–2896.